Paper Number

Measurements of the space radiation environment with REM

Paul Bühler, Laurent Desorgher, and Alex Zehnder
Paul Scherrer Institute, 5232 Villigen PSI, Switzerland

Alexi Glover
Mullard Space Science Laboratory, Holmbury St. Mary, Dorking, Surrey RH5 6NT, United Kingdom

Eamonn Daly
ESA/ESTEC, 2200 AG Noordwijk, The Netherlands

Copyright © 2000 Society of Automotive Engineers, Inc.

ABSTRACT

We compare measurements of the space radiation environment from particle detectors aboard Mir and Strv-1b (Geostationary Transfer Orbit) with the NASA AE8/AP8 radiation belt models. The two orbits cover a large area of space, which allows to test the standard models in a number of key regions and point out their deficiencies.

INTRODUCTION

To describe the proton and electron fluxes in the earth's radiation belts, most commonly the AE8/AP8 models are used [1,2]. They were build with data from the 1960`s and 70`s. There are versions for solar minimum and solar maximum, but otherwise the models are static. There are a number of shortcomings of the models, of which the most obvious are the fact that they do not describe any variations and that they have not been updated with new data since their creation (for a discussion of the models see e.g. http://www.estec.esa.nl/wmwww/WMA/ecss.html)

An update of the models is highly desirable. The interest of the community in new standard models has lead to the establishment of the COSPAR Panel on Standard Radiation Belts. The goal is the development of a new standard model of the Earth's trapped radiation belts (http://cospar.itodys.jussieu.fr/scistr/psrb.html).

In this paper we compare recent measurements of the radiation environment in an equatorial Geostationary Transfer Orbit, GTO and in a Low Earth Orbit, LEO with the NASA models. Both orbits are of special interest. LEO is the preferred orbit for manned space missions (Mir, Space Shuttle, ISS) and covers the South Atlantic Anomaly, SAA. GTO experiences the most severe environment, because it samples the equatorial region, and also samples Geostationary Orbit, GEO, which is the most populated region in space.

With this paper we intend to make a contribution to the awaked discussion about the construction of new standard radiation belt models, by pointing out the limits of the present 'standard'.

DATA AND METHOD

DATA

We used data from the two Radiation Environment Monitors, REM [3] aboard the UK satellite Strv-1b and the Russian space station Mir. The two instruments are identical except for the shielding as shown in table 1.

The REM instrument consists of two independent shielded silicon detectors and measures the energy deposit, ΔE of charged particles. Energy deposits from 1 Mip to more than 1000 Mips (1 Mip $\approx$ 117 keV) are registered and counted into 16 channels per detector head. The instruments are operated in integral mode; data is accumulated for between 30 and 1000 seconds, depending on mission and orbit position. The aperture of the instrument is defined by an aluminium cone with an opening angle of 90°. Both detectors are covered with a dome of aluminium which defines the lower energy threshold for particles to reach the sensitive detector part to approximately 1 MeV for electrons and 25 MeV for protons in the case of the Strv-REM, and 0.5 MeV and 10 MeV, in the case of Mir-REM. One of the detector heads has an additional shielding of tantalum, which significantly reduces the penetration of electrons for this detector. It is therefore called p-detector, whereas the other one is denoted as e-detector. The resulting shielding over the aperture is listed in table 1. Outside

the aperture the shielding is not perfect and especially high-energy protons can penetrate from the sides. The shieldings listed in table 1 are therefore to be taken as lower limits.

Strv-1b was in a 10.5h Geostationary Transfer Orbit, GTO with an inclination of 7°, an apogee of 250 km, and a perigee of 36000 km. It was spinning with a rate of 6.5 rpm. The space station Mir is in a 90-minute, nearly circular orbit at 420 km altitude and an inclination of 52°. Data from REM aboard Strv-1b is available for August 1994 to September 1998 and from REM aboard Mir, for November 1994 to December 1996.

Table 1: Shieldings of the REM detectors aboard the UK satellite Strv-1b and the Russian space station Mir.

Mission	Detector	Shielding [g/cm^2]
Strv-1b	p-detector	>2.06
	e-detector	>0.81
Mir	p-detector	>2.06
	e-detector	>0.20

The NASA models were accessed with the UNIRAD suite from BIRA/BISA [4]. This software allows to control the access with a number of parameters. Important here are the geomagnetic and external magnetic field models for which we selected the IGRF95 and the Tsyganenko 96 at geomagnetic quiet conditions (KP = 0). The same magnetic field models were also used to calculate the magnetic field, B and L-shell parameter, L, used throughout this paper. UNIRAD allows to correct for the secular drift of the magnetic field by a westward rotation of the SAA of 0.3°/yr [5]. This correction is applied in our calculations. 1995/1996 was at the end of the declining phase of the solar cycle 22, close to solar minimum, which reached its minimum in fall 1996. We therefore used the solar minimum version of NASA models to compare with REM data.

AE8/AP8 are omnidirectional models. Considering the large opening angle of REM and the long accumulation times compared to the spinning rate of the satellite, the Strv-REM observations can be assumed to represent the omnidirectional particle fluxes. For Mir-REM the situation is different, because during the accumulation time of 32 sec the space station was normally not changing orientation. However, during the two years lifetime all orientations were fairly homogeneously sampled and therefore the mission-averaged data can be assumed to represent the omnidirectional environment.

METHOD

In order to test the NASA AE8/AP8 models we computed the expected response of the REM detectors to the model spectra and compared the such simulated detector signals with the measurements. In order to reduce the amount of data points to compare, the observations were binned into B-L-bins, and averaged over time. For the NASA models we extracted for each B-L-bin the respective proton and electron differential spectra, fp(E) and fe(E), and calculated the expected REM count rates, c_i. Count rates in units of counts/sec and incident particle spectra in units of 1/cm2/sec/MeV are related by

$$c_i = \int_0^\infty \left(f_e \cdot G_e(i,E) + f_p \cdot G_p(i,E) \right) dE \qquad (1)$$

where index i denotes the detector channel and runs from 1 to 32 (channels 1 to 16 are p-detector and channels 17 to 32 are e-detector). The geometric factors Gp,e(E) in units of cm^2 were determined by calibration measurements and MonteCarlo simulations. Count rates can be transformed to dose rates by multiplying the count rates in each channel with the respective channel-average energy deposit. By summing the dose rates over a number of channels we obtain a quantity which we denote by restricted dose. The adjective 'restricted' is used here because we omit the lowest detector channels in the sum since they are partly contaminated with electronic noise, and also the highest channel, because it only contains events from cosmic rays.

Figure 1 shows a colour map of the time-averaged measured restricted dose rates as function of B and L. In this figure data from both satellites are combined. The lower narrow branch of coloured area is from Strv-1b and the upper branch from Mir. Light colours represent high doses and dark colours, low doses. Both orbits cover the L-range from approximately 1 to 7 RE but at different magnetic latitudes. Note, that between L=1 and 1.5 RE the data sets partly overlap. The upper panel shows the restricted dose rates in the e-detectors and the lower panel, those in the p-detectors. The grey coloured area is not covered by the two satellites.

The map reveals the typical features of the high-energy tail of the radiation environment. There is the inner zone at $L \leq 2.5$ RE, which is dominated by protons, the outer zone at $L \geq 3.5$ RE, which is dominated by electrons, and the slot region between the two belts. Note that in the outer zone the dose rates in the p-detector are much lower than in the e-detector, proofing the efficient shielding of the electrons by the tantalum layer of 0.75 mm.

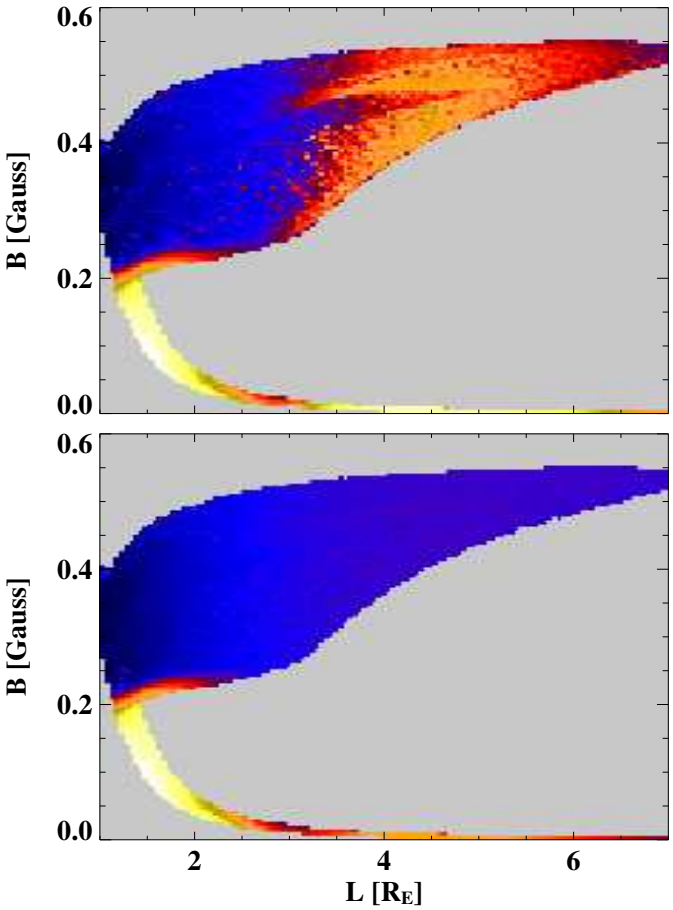

Figure 1: Colour map of the restricted dose rates in the REM detectors aboard Strv-1b (lower branch of coloured area) and aboard Mir. The upper panel shows p-detector data and the lower panel, data from the e-detectors.

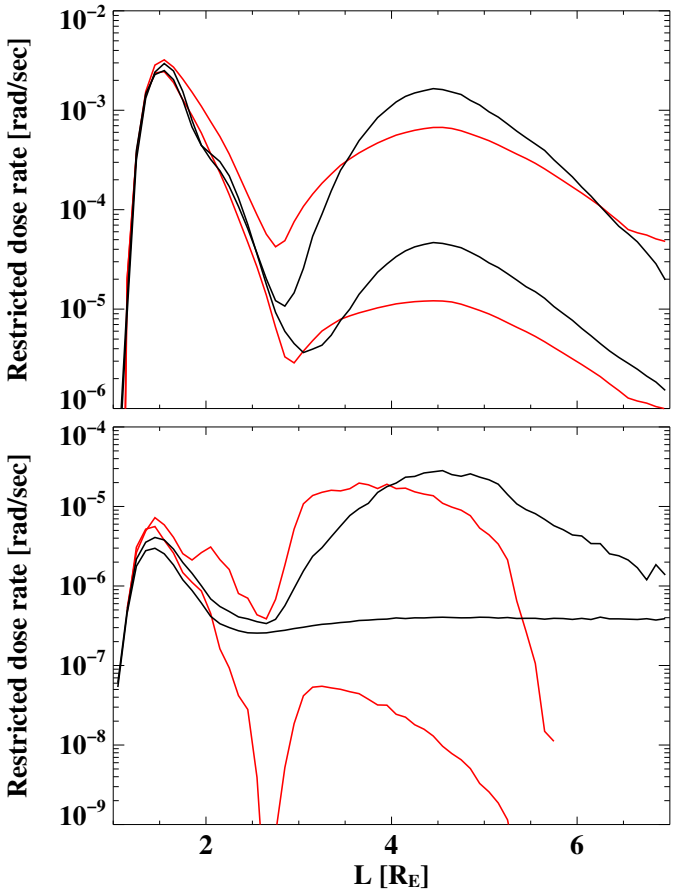

Figure 2: B-averaged restricted dose rates a function of L. The upper panel shows Strv-REM data and the lower panel, Mir-REM data. Red lines represent model predictions and black lines, the measurements.

The B-dependence of the dose rates reflects the pitch angle distribution of the particle fluxes. At a given L the dose rates decrease with increasing magnetic latitude. In the inner zone there is obviously a rather sharp fall-off at around B ≈ 0.2 G, which corresponds to $B/B_0 \approx 2.2$, where B_0 is the equatorial magnetic field strength, or an equatorial pitch angle, α_0 of approximately 50°. Although the dose rates in the outer zone do also decrease with magnetic latitude, the decrease is less steep than in the inner zone, indicating a flatter pitch angle distribution for the outer zone electrons compared to the inner zone protons.

MODEL VERSUS MEASUREMENTS

In a first step we compare the B-averaged measured and predicted restricted dose rates, which are plotted in figure 2. The upper panel shows Strv-1b data and the lower panel, the Mir data. The red lines are the model predictions and the black lines the measured values. The curves with the higher dose rates in the outer belt are the e-detector data and the lower curves are the p-detector data. The data was averaged over 2 years, August 1994 to August 1996 in the case of Strv-1b and November 1994 to November 1996, in the case of Mir.

At the inner edge of the inner radiation belt (L < 1.5 RE), measurement and model predictions compare very well. But at the outer edge of the inner belt and in the outer radiation zone there are significant differences between measurements and predictions.

In the following we will address the critical regions in some detail.

INNER RADIATION BELT

1.0 < L < 1.5 RE

Figure 2 suggests that the NASA models do well describe the environment in this region. A more detailed analysis confirms this impression but also reveals some limits. In figure 3 the restricted dose rates at 1.35 < L < 1.40 RE are plotted as function of B. The left panel

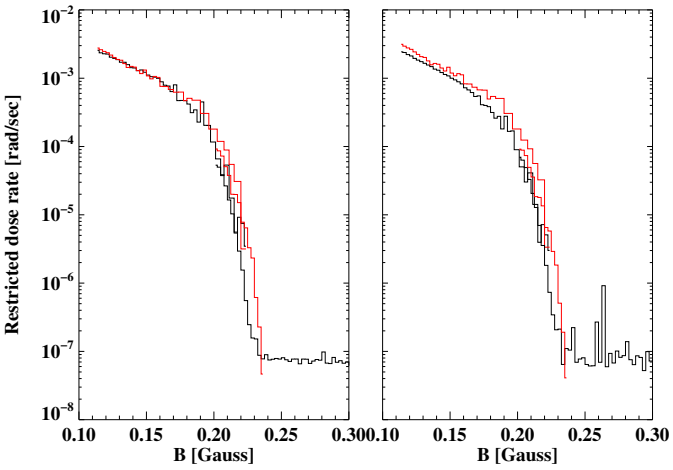

Figure 3: Restricted dose rates at 1.35 < L < 1.4 RE versus B. Left and right panel show p-detector and e-detector data, respectively. The black line represents the measured values and the red line, the model predictions.

shows p-detector data and the right panel e-detector data. The black lines are REM data and the red lines the model predictions. In this figure Strv-1b and Mir data are combined and overlap at 0.20 < B < 0.22 G. However, the two data sets can not be expected to perfectly match because of the different total shielding of the detectors aboard Mir and Strv-1b. Below B = 0.16 G the relative difference between model and STRV-1b measurements is less than 10% in the p-detector and less than 40% in the e-detector, which is presumably within the uncertainty range of the applied geometric factors. The difference increases towards higher B-values and reaches approximately 70% and 100%, respectively at B = 0.2 G, the region, where the Mir data start. There the model predictions are systematically higher than the measurements. At B > 0.23 G the observed restricted dose rate levels out, whereas the model drops to 0. In this region the observations are dominated by cosmics, which of course are not modelled with AE8/AP8.

PROTON SPECTRA

So far we compared doses. But with REM it is also possible to estimate the spectra of the incident protons and electrons. The differential proton spectra are therefore approximated by a power law, fp(E)=fp0(E/Ep0)^γp, and the electron spectra by an exponential function, fe(E)=fe0exp(-γe(E-Ee0)). The free parameters fp0, γp, fe0, and γe, are determined by fitting the measured count rates with the relation given in equation 1. Ep0 and Ee0 are fixed to 30 MeV and 1 MeV, respectively. Reliable results are obtained where the contribution of either particle species to the count rates is statistically significant. In the inner belt the contribution of electrons to the REM counts is small compared to the protons and the electron spectra are therefore not well defined by the REM measurements. But for the protons the spectral parameters can be deduced and compared with the NASA model spectra, which for this purpose are also fitted with a power law function.

In table 2, γp is listed for a number of B-L-bins. The two B-values per L-value correspond to the respective minimum magnetic field bin encountered by the two satellites. In the lowest L-bin the low Mir count rates do not allow to extract the spectrum.

Both, model and measurements show that in the region between 1.0 < L < 1.5 RE the spectral index γp is an increasing function of L and decreases with B (the proton spectra become softer with increasing L and harder with increasing magnetic latitude). Considering the simplifying power law approximation and the statistical uncertainties of the fitted values (≥ 25%, depending on bin), we note, except at very low L-values a rather good agreement between the model and measured spectral indices. At L < 1.2 RE the NASA spectra are considerably softer than the measured spectra. Inspection of the energy deposit histograms in this region indeed shows, that there are many low ΔE-events in both, p- and e-detector, which are a sign for the presence of very energetic protons, and which are not produced by the soft NASA spectra.

Table 2: Proton power law spectral index γp for a number of B-L-bins at the inner edge of the inner radiation belt.

L [RE]	B [G]	γp model / REM
1.10 - 1.15	0.21 - 0.22	2.00 / 0.81
1.20 - 1.25	0.16 - 0.17	0.79 / 1.01
	0.19 - 0.20	0.49 / 0.96
1.30 - 1.35	0.13 - 0.14	1.16 / 1.13
	0.20 - 0.21	1.08 / 1.04
1.40 - 1.45	0.11 - 0.12	1.38 / 1.24
	0.20 - 0.21	1.14 / 1.21
1.50 - 1.55	0.08 - 0.09	1.78 / 1.61
	0.21 - 0.22	1.12 / 1.37

1.5 < L < 2.5 RE

At 1.5 < L < 2.5 RE the measured and predicted L-distributions of the dose rates show significant differences (see figure 2). The Strv-data curve has a hump at L ≈ 2 RE, which is not present in the model, and the predicted Mir e-detector doses have a feature at approximately the same L-position, but which is not measured.

The peak at L = 2.0 RE in the Mir model curve is a feature of the <30 MeV protons in the NASA models. The flux L-distribution of these low energy protons has a secondary peak there. The fact that this is only present at lower energies explains why it is only seen in the predicted restricted dose rates of the e-detector. This is a model feature, which is not compatible with the observations.

Comparing the predicted and measured ΔE-histograms in this region we note that the measured histograms are biased towards lower ΔE-channels, compared to the modelled histograms, in all, Strv-1b and Mir detectors. This is a strong indication for the true proton spectra to be significantly harder than the NASA model spectra. In table 3 the power law spectral indices for a number of B-L-bins at the outer region of the inner belt are compared. At L > 1.8 RE the difference between model and REM values becomes significant. Both, model and REM spectra soften with L, but the model spectra with a much steeper gradient.

Although the particle fluxes are normally very stable in this region, it can happen that during large magnetic storms particles are injected into this region, as it happened in March 91 [6]. Much earlier already McIlwain [7] has noted a secondary peak in the proton distribution at L ≈ 2.2 RE, which slowly decayed and moved inward with time. It is probable that the remainder of the March 1991 event causes the differences we observe.

Table 3: Proton power law spectral index γp for a number of B-L-bins at the outer edge of the inner radiation belt.

L [RE]	B [G]	γp model / REM
1.60 - 1.65	0.07 - 0.08	2.09 / 1.91
	0.21 - 0.22	1.25 / 1.53
1.80 - 1.85	0.05 - 0.06	2.58 / 2.05
	0.22 - 0.23	2.12 / 1.75
2.00 - 2.05	0.03 - 0.04	3.21 / 2.18
	0.22 - 0.23	2.68 / 1.97
2.20 - 2.25	0.02 - 0.03	3.77 / 2.26
	0.23 - 0.24	4.01 / 2.07
2.50 - 2.55	0.01 - 0.02	4.83 / 2.52

SAA

The SAA is located at the geographic region, where, at a given altitude, the magnetic field strength is minimum. Since the SAA is linked with the magnetic field distribution, it is subjected to a westward drift, which is associated with the secular drift of the earth's magnetic field. When using the NASA models this is taken into account by adding a value of 0.3°/yr to the geodetic longitude before calculating the B and L which are then used to access the model spectra. Figure 4 shows a

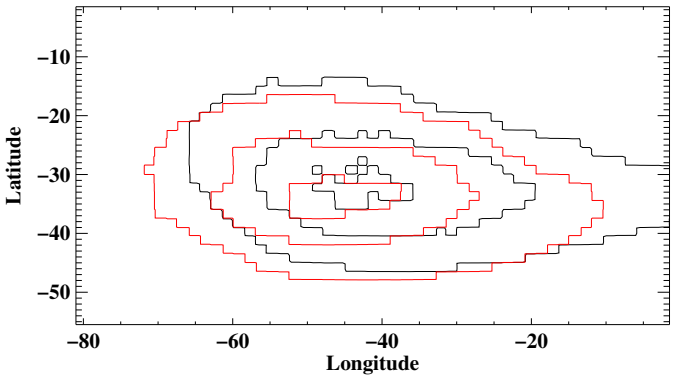

Figure 4: Contour plot of the restricted dose rate in the p-detector aboard Mir (black lines) in the SAA. The contour levels are 10%, 50%, and 90% of the value at –43° longitude and –32° latitude. The red lines show the model predictions.

contour plot of the measured (black lines) and model predicted (red lines) restricted dose rates in the p-detector aboard Mir. The three contour lines are the 10%, 50%, and 90% levels of the dose rate value at –43° longitude and –32° latitude, the position of the measured maximum. The model contours are obviously shifted west compared to the measured contours. The correction applied in the model seems to overestimate the true drift. At a given point in space this may lead to an over- or underestimation of the environment. But over a longer period, e.g. a mission lifetime, the region is homogeneously sampled, and such a displacement of he SAA location has little effect on the estimated total dose.

We justified to assume the Mir-observations to represent the omnidirectional environment by using long-term averages. In the SAA however, the proton fluxes are anisotropic [8]. This can be demonstrated by sorting the Mir data according to the orientation of the detector aperture [9]. It was shown that the proton fluxes arriving from east in the SAA are lower and have a softer spectrum than the protons arriving from west. The east-west ratio is a decreasing function of L and vanishes above L ≈ 1.7 RE.

Temporal variations

The inner belt proton fluxes are known to be subjected to solar cycle variations. The strength of the source and

loss processes is a function of solar cycle resulting in high proton levels at solar minimum and low levels at solar maximum [10]. The effect is most pronounced at low L, high magnetic latitude, and high energies.

For the Strv-REM detectors the solar minimum and maximum versions of the NASA models yield no difference in the predicted restricted doses. But at Mir latitude the difference is significant. At L= 1.2 RE for example, the solar minimum version gives by a factor 20 higher restricted dose rates than the solar maximum version.

From the four REM detectors it is the p-detector aboard Mir with which it is most probable to observe these variations. And indeed the variations over the two years of operation, of the restricted dose rate in the SAA follow the solar irradiance variations [11]. A general increase of the SAA doses during 1995 by approximately 25% coincided with a simultaneous decrease of the solar irradiance. An enhanced solar irradiance leads to a heating of the earth's upper atmosphere, which at a given altitude results in an increase of the atmospheric density and subsequent enhanced absorption of protons at the mirror points. The observation period of 2 years is too short to trace the solar cycle variation, which however has been shown to be important [12].

OUTER RADIATION BELT

In the region between 3.0 < L < 7.0 RE the deviations of the model predictions from the measurements are important (see figure 2). The p-detector aboard Mir is dominated by cosmics and can therefore not be used to judge the model. But the Mir e-detector shows that the model electron fluxes vanish above L ≈ 5.5 RE, which is not observed. At the Strv-1b orbit the model gives a smooth L-distribution of the restricted dose rates but also deviates considerably from the observations. This is not surprising if we recall the fact, that the outer belt is very dynamic and thus can hardly be accurately described by static models as the NASA AE8/AP8 are. In figure 5 the average restricted dose rates per outer belt passage (3.5 < L < 7.0 RE) in the Strv e-detector is plotted versus time (dashed line). The horizontal bold black line shows the mission averaged REM rate and red line, the model prediction. Between the minimum and maximum measured values there is more than a factor 1000! It may therefore be surprising, that the difference between model and averaged measured values is only a factor 2 or so. However, this ratio depends on the period over which the average is computed. Over the first year of the mission the average dose rate is a factor 5 higher than over year 1997, for example.

The large variations are triggered by fast solar wind streams. At the relativistic electrons the arrival of such a wind stream at the magnetopause normally causes a typical sequence of first decaying and after a few days more or less strongly increasing fluxes [13]. The electron flux variations are accompanied by spectral changes. Although it is known that fast solar wind streams are requisite for these variations, the exact mechanism leading to the observed electron flux enhancements is not fully understood and a subject of active debate [e.g. 14]. There is also a semi-annual modulation observed. This is demonstrated with the bold black curve in figure 4, which shows the 3-month running average of the measured e-detector restricted

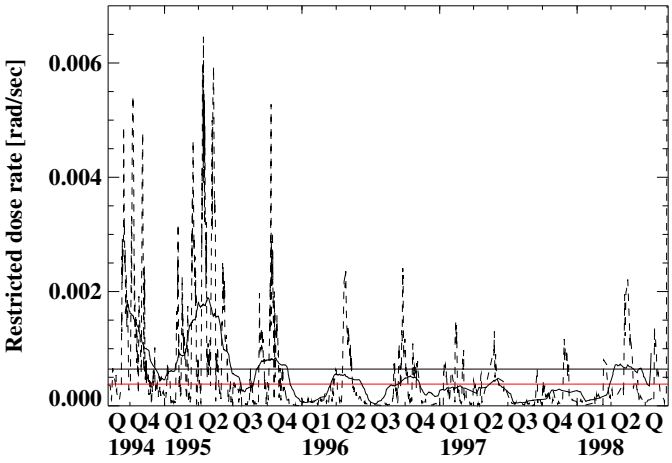

Figure 5: Average restricted dose rates in the Strv e-detector per outer radiation belt passage (3.5 < L < 7.0). The dotted curve shows the per passage data and the bold curve a three-month running average. The black horizontal line is the total average and the red line, the model predicted value

doses. The doses are high during spring and fall and low during winter and summer. These variations are not observed in the solar wind and are caused by a semi-annual modulation of the process responsible for the electron enhancements [15].

Besides the large and fast variations the outer belt is always subjected to slower diffusion and loss process, which during geomagnetic quiet times let the electron fluxes decay, the spectra harden, and the peak of the L-distribution move inward.

Instead of using one static model to describe the outer belt environment, attempts are made, to make models depend on geomagnetic activity or solar wind conditions. CRRESELE is a set of models for a number of AP15 ranges (Ap15 is the 15-day average of Ap) [16]. The models were build with data from the CRRES satellite, and are therefore only valid for the specific GTO. They show that the environment becomes more severe with increasing AP15. In these models AP15 is used for the entire outer belt. But the variations at large L are normally faster and larger than deeper in the magnetosphere. A study on the L-dependence of the variations has shown [17] that at L ≈ 4.5 RE AP15 is a

good parameter to describe the electron fluxes but that e.g. at GEO the 3-day averaged solar wind speed gives much better correlation than AP15.

CONCLUSION

The comparison of REM observations with the NASA AE8/AP8 models shows that there are considerable differences between the model predictions and measurements. However, whether a model is accepted to be sufficiently accurate or not probably depends on the kind of problem it is applied for. For a long-term technical mission an overall factor of 5 in the miss-prediction of the absorbed dose may be acceptable but for shorter term, especially manned missions it would certainly be preferable to have a more accurate estimate. Some specific applications need dedicated models. To assess the vulnerability of satellites to electrostatic charging e.g. rather a worst case model than an average model is needed [18].

New models should aim to reach the highest possible reliability. Important inputs to the modelling process are accurate data sets and a theoretical understanding of the radiation belt physics. Simple instruments like REM can make valuable contributions. The data can be used to validate models and theories (as shown here), monitor changes of the environment, and also to build new models.

ACKNOWLEDGMENTS

This work was supported by ESA's Technology Research Program under the Space Environments and Effects Major Axis, ESA/TOS-EMA.

REFERENCES

1. Vette, J.I., The AE-8 trapped electron environment, NSSDC/WDC-A-R&S 91-24, 1991

2. Sawyer, D.M. and Vette, J.I., AP-8 trapped proton environment for solar maximum and solar minimum, NSSDC/WDC-A-R&S 76-06, 1976

3. Bühler, P., Ljungfelt, S., Mchedlishvili, A., Schlumpf, N., Zehnder, A., Adams, L., Daly, E., and Nickson, R., Radiation environment monitor, *Nucl. Instr. And Meth. In Phys. Res. A 368*, 825, 1996

4. Heynderickx, D., Kruglanski, M., and Lemaire, J., UNIRAD v3.0, Trapped Radiation Software, Belgian Institute for Space Aeronomy, 1180 Brussels, Belgium, 1996

5. Heynderickx, D., Comparison between methods to compensate for the secular motion of the Sout Atlantic Anomaly, Rad. Mes., 26, 369, 1996

6. Blake, J.B., Kolasinski, W.A., Fillius, R.W., and Mullen, E.G., Injection of electrons and protons with energies of tens of MeV into L<3 on March 24, 1991, Geophys. Res. Lett., 19, 821, 1992

7. McIlwain, C.E., J. Geophys. Res. 71, 3623, 19666

8. Sakaguchi, T., Doke, T, Hasebe, N. et al., Measurements of the directional distribution of incident particles in the Shuttle-Mir mission orbit, J. Geophys. Res. 104, 793, 1999

9. Bühler, P., Zehder, A., Kruglanski, M., Daly, E.., Energy and spatial dependence of the east-west effect observed by Mir-REM, SREW conference, Farnborough, 1999

10. Albert, J.M., Ginet, G.P., Gussenhoven, M.S., CRRES observations of radiation belt protons 1. Data overview and steady state radial diffusion, J. Geophys. Res. 103, 9261, 1998

11. Bühler, P., Desorgher, L., Zehnder, A., Daly, E., and Adams, L., REM measurements aboard Mir during 1995, *Adv. Space Res., 21*, 1645, 1998

12. Huston, S., and Pfitzer, K., A new model for the low altitude trapped proton environment, I*EEE Nucl. Sci. Rad. Effects Conference*, July, 1998

13. Desorgher, L., Bühler, P., Zehnder, A., Daly, E., and Adams, L., Outer radiation belt variations during 1995, Adv. Space Res., 22, 83, 1998

14. Rostoker, G., Skone, S., and Baker, D.N., On the origin of relativistic electrons in the magnetosphere associated with some geomagnetic storms, Geophys. Res. Lett. 25, 3701, 1998

15. Baker, D.N., Kanekal, S.G., Pulkinnen, T.I., and Blake, J.B., Equinoctial and solstitial averages of magnetospheric relativistic electrons: A strong semiannual modulation, Geophys. Res. Lett. 26, 3193, 1999

16. Brautigam, D.H. and Bell, J.T., CRRESELE Documentation, Tech. Rep. PL-TR-95-2128, Phillips Laboratory, Hascom Ait Base, MA 01731-3010, 1995

17. Bühler, P., Desorgher, L., Zehnder, A., Kruglanski, M., Quaghebeur, B., and Daly, E., Geomagnetic and solar wind parameters to predict the relativistic electron fluxes in the outer radiation belt, SREW conference, Farnborough, 1999

18. Wrenn, G.L., Rodgers, D.J., and Bühler, P., Modelling the outer belt enhancements of MeV electrons, J. Spacecraft and Rockets, 2000

CONTACT

Dr. Paul Bühler, paul.buehler@psi.ch